23rd International Congress on Sound & Vibration
Athens, Greece 10-14 July 2016
ICSV23

TOWARDS LARGE AEROACOUSTIC APPLICATIONS THROUGH A HYBRID APPROACH BASED ON THE LINEARIZED EULER EQUATIONS

Legendre, C.; de Brye, B.; Subramaniyam, S.; Ganty, B.; Detandt, Y.
Free Field Technologies S.A. www.fft.be, Axis Park Louvain-La-Neuve, Rue Emile Francqui 9, B-1435 Mont Saint Guibert, Belgium, email: cesar.legendre@fft.be

Bailly, C.
Laboratoire de Mécanique des Fluides et d'Acoustique, Ecole Centrale de Lyon & UMR CNRS 5509, 36 avenue Guy de Collongue, 69134 Ecully cedex, France

For low Mach number applications, the acoustic and fluid dynamics physical phenomena are very disparate in terms of characteristic length and energy scales. In the hybrid approach proposed in this paper, the turbulent unsteady flow solution is processed in order to determine equivalent noise sources. These are considered as the forcing terms for the Linearized Euler Equations (LEE), which are solved to obtain the acoustic field. The acoustic propagation is computed using a high-order adaptive discontinuous Galerkin (DG) scheme in the time domain. Frequency domain results are obtained through a discrete Fourier transform. The choice of high-order DG methods for solving the LEE in the time domain present the advantages of: (i) the element interpolation can be locally increased to accurately represent the phenomena, i.e. propagation and source representation; (ii) the numerical method has a high parallel scalability and, therefore, suited to large acoustic problems with an acceptable computational cost. In the present work, the solution for a low Mach ($M < 0.1$) simplified HVAC duct with a rectangular cross section is presented. Even if the size of the model does not specifically require the usage of the LEE or DG methods, this configuration is compared to a solution provided by an aeroacoustic solver already extensively validated and dedicated to acoustically compact problems. Finally, the numerical results are also compared to equivalent solutions obtained through a finite-element based discretization of Lighthill's analogy.

1. Introduction

The theory of aerodynamic generated sound has been constantly reviewed over the last six decades. All this started with Lighthill [1, 2] who defined the concept of acoustic analogy as a reformulation of the fluid dynamics equations into a form of a wave operator in l.h.s (left-hand side) and the remaining terms on the r.h.s (right-hand side) as the sound sources produced by turbulence. As stated by Doak[3], Lighthill's analogy is a set of equivalent quadrupole sources computed by means of fluid dynamics equations that are propagated in a fictitious but convenient fluid at rest. The quadrupole sources are expressed as second spatial derivatives of Lighthill's tensor $\partial^2 \mathbf{T}_{ij}/\partial x_i \partial x_j$, where $\mathbf{T}_{ij} = \rho v_i v_j + \delta_{ij}(p - c^2\rho) - \boldsymbol{\tau}_{ij}$. The wave propagation is governed by d'Alembert's operator applied to the fluctuating density, i.e. $\frac{1}{c^2}\frac{\partial^2}{\partial t^2} - \boldsymbol{\nabla}^2$. This corresponds to an hybrid approach in which the flow is computed first and the noise sources are extracted and then propagated in a second step. Further improvements and modifications to Lighthill's theory have been added in both sides of the

equation, the left-hand side (operator) and the right-hand side (sources). For instance: (i) Curle [4] took into account solid boundaries effects; (ii) Ffowcs-Williams & Hawkings [5] considered solid boundaries and uniform convection effects; (iii) Ribner [6] proposed aerodynamic source terms proportional to the first derivative in time of the turbulent pressure fluctuations; (iv) a third-order operator was proposed by Lilley [7] to take into account the effects of non-uniform flows with vorticity; and (v) Howe [8], Doak [3] and Möhring [9] proposed acoustic analogies based in convected wave operators for arbitrary but potential flows in terms of the total enthalpy with turbulent, entropic and temperature sources.

Since the large majority of acoustic analogies requires the aerodynamic information as input data, the progress of computational fluid dynamics (CFD) is closely linked with aeroacoustics[10]. The advance of computational methods in fluid dynamics has increased the quality and complexity of the aerodynamic information available and therefore the source predictions. Likewise, the operator used in the acoustic analogies has evolved from scalar to vector operators, i.e. the linearised Euler (LEE) or linearised Navier-Stokes equations (LNSE). There are two main reasons: (i) the rich variety of effects over the wave motion, i.e. classic convection, mean vorticity, thermal and viscous effects among others; and (ii) the fact that they are well-adapted to high efficient and parallelizable numerical methods such as discontinuous Galerkin (DG) method. For instance, (i) Bogey *et al.* [11] have imposed aerodynamic sources to the momentum equation in the LEE; (ii) Billson *et al.* [12] by using Favre's decomposition of variables included sources on the momentum and energy equations of the LEE in conservative form; (iii) Goldstein [13] starting from the Navier-Stokes equations formulated a modified form of the LEE using auxiliary variables with sources in the momentum and energy equations; and (iv) Ewert *et al.* [14] have proposed a family of acoustic perturbation equations (APE) with mass, momentum and energy sources.

The present article describes an efficient implementation of the LEE using a high-order adaptive DG scheme in time domain [15], with aeroacoustic sources imposed on the right-hand side of the momentum equation (Section §2). The sources are computed from time-dependent CFD results using *OpenFOAM* (Section §3), while *ActranDGM* is used as the acoustic solver (Section §2). Since the DG method operates with large-size elements of high $p-$order interpolation, the aerodynamic sources are sub-sampled inside the element to take into account the small turbulent scales present in comparison to the wavelength of the problem. As numerical reference, the present method is compared to equivalent solutions obtained through a finite-element (FE) based discretization of Lighthill's analogy, using *Actran* [22] in frequency domain (Section §4). The advantages that represent the implementation of an hybrid approach in time domain for aeroacoustics (LEE with sources) in a DG context are the following: (i) the p-adaptivity allows to use the same mesh for different frequencies adjusting dynamically the elements' order; (ii) to explore new physics in propagation and generation of sound using the LEE, i.e. mean flow with vorticity, propagation and coupling of entropy and vorticity waves with acoustics; and (iii) high parallel scalability suited to large acoustic problems and high frequency, characteristic of industrial problems. The case study selected for this work is a simplified HVAC (***H**eating, **V**entilation, and **A**ir **C**onditioning*) system consisting of a duct with rectangular cross section and a 90° bend as depicted in figure 1a. This case has been extensively discussed in the literature [16, 17]. Finally the results are discussed and analysed (Section §5) followed by some concluding remarks and possible further investigations (Section §6).

2. Theory

Considering the vector of variables $\boldsymbol{q}$, the flux matrix $\mathbb{F}$, a matrix gradient $\boldsymbol{s}$ and the vector of sources $\mathbb{R}$, the isentropic linearised Euler equations with source terms may be written in the following compact form:

$$\frac{\partial \boldsymbol{q}}{\partial t} + \frac{\partial}{\partial x_j}\left(\mathbb{F}_j.\boldsymbol{q}\right) - \boldsymbol{s}.\boldsymbol{q} = \mathbb{R}, \tag{1}$$

in which $\boldsymbol{q}$ contains the fluctuating density, velocity and pressure, $\boldsymbol{q} = [\rho, u, v, w, p]$ and:

$$\mathbb{R} = \begin{bmatrix} 0 \\ \left(R_1 - \bar{R}_1\right)/\rho_0 \\ \left(R_2 - \bar{R}_2\right)/\rho_0 \\ \left(R_3 - \bar{R}_3\right)/\rho_0 \\ 0 \end{bmatrix}, \quad \mathbb{F}_j = \begin{bmatrix} v_j^0 & \rho_0\delta_{1j} & \rho_0\delta_{2j} & \rho_0\delta_{3j} & 0 \\ 0 & v_j^0 & 0 & 0 & \frac{\delta_{1j}}{\rho_0} \\ 0 & 0 & v_j^0 & 0 & \frac{\delta_{2j}}{\rho_0} \\ 0 & 0 & 0 & v_j^0 & \frac{\delta_{3j}}{\rho_0} \\ 0 & \rho_0 c^2\delta_{1j} & \rho_0 c^2\delta_{2j} & \rho_0 c^2\delta_{3j} & v_j^0 \end{bmatrix},$$

$$\boldsymbol{s} = \begin{bmatrix} 0 & 0 & 0 & 0 & 0 \\ \frac{1}{\rho_0^2}\frac{\partial p_0}{\partial x} & \frac{\partial v_j^0}{\partial x_j} - \frac{\partial u_0}{\partial x} & -\frac{\partial u_0}{\partial y} & -\frac{\partial u_0}{\partial z} & -\frac{1}{\rho_0^2}\frac{\partial \rho_0}{\partial x} \\ \frac{1}{\rho_0^2}\frac{\partial p_0}{\partial y} & -\frac{\partial v_0}{\partial x} & \frac{\partial v_j^0}{\partial x_j} - \frac{\partial v_0}{\partial y} & -\frac{\partial v_0}{\partial z} & -\frac{1}{\rho_0^2}\frac{\partial \rho_0}{\partial y} \\ \frac{1}{\rho_0^2}\frac{\partial p_0}{\partial z} & -\frac{\partial w_0}{\partial x} & -\frac{\partial w_0}{\partial y} & \frac{\partial v_j^0}{\partial x_j} - \frac{\partial w_0}{\partial z} & -\frac{1}{\rho_0^2}\frac{\partial \rho_0}{\partial z} \\ 0 & \rho_0\frac{\partial c^2}{\partial x} & \rho_0\frac{\partial c^2}{\partial y} & \rho_0\frac{\partial c^2}{\partial z} & \frac{c^2}{\rho_0}v_j^0\frac{\partial \rho_0}{\partial x_j} + \frac{\partial v_j^0}{\partial x_j} \end{bmatrix}. \tag{2a-c}$$

Where the aerodynamic source R applied to the momentum equation is defined by:

$$R_j = -\frac{\partial \rho v_i v_j}{\partial x_i}, \quad \overline{R}_j = -\overline{\frac{\partial \rho v_i v_j}{\partial x_i}}. \tag{3a,b}$$

The index "0" denotes the mean flow, sub-index is used for the mean flow pressure p_0 and density ρ_0, super-index for the mean flow velocity v_j^0. The speed of sound is denoted by c while δ_{ij} is Kronecker's delta. Furthermore, the expression of the aerodynamic sources (2a;3a,b) is found by analogy with Lighthill's equation [1] in the case of no flow or Lilley's equation [7] in the case of unidirectional shear flow [11]. Besides, the source term (2a) is assumed to be known, non-linear and their mean values are subtracted. In contrast to second-order scalar operators used in well-known acoustic analogies [1, 3, 8, 9], the LEE does support the presence of vortical and entropy waves [18, 19]. These waves are completely absent or decoupled from pressure waves: in a medium at rest, or with constant convection or in presence of a potential mean flow. The same waves are coupled to acoustics in the case of arbitrary mean flows with vorticity. Additionally, the source term $\mathbb{R}$ may contain vortical and entropy waves that in a vortical mean flow can rapidly grow causing physical instabilities (Kelvin-Helmholtz) and therefore polluting the solution.

2.1 Numerical Method

Considering equation (1) being multiplied by the Lagrange high-order polynomial shape functions $\mathbf{N}_\alpha$ and integrated over the volume Ω, this results in:

$$\int_\Omega \mathbf{N}_\alpha \frac{\partial \boldsymbol{q}}{\partial t} \mathrm{d}\Omega + \int_\Omega \mathbf{N}_\alpha \frac{\partial}{\partial x_j}\left(\mathbb{F}_j.\boldsymbol{q}\right)\mathrm{d}\Omega - \int_\Omega \mathbf{N}_\alpha \boldsymbol{s}.\boldsymbol{q}\mathrm{d}\Omega = \int_\Omega \mathbf{N}_\alpha \mathbb{R}\mathrm{d}\Omega. \tag{4}$$

Integrating by parts the second term of equation (4) to transfer the derivative in space $\partial/\partial x_j$ to the shape functions $\mathbf{N}_\alpha$, equation (4) results in:

$$\int_\Omega \mathbf{N}_\alpha \frac{\partial \boldsymbol{q}}{\partial t} \mathrm{d}\Omega = \int_\Omega \frac{\partial \mathbf{N}_\alpha}{\partial x_j}\mathbb{F}_j.\boldsymbol{q}\mathrm{d}\Omega + \int_\Omega \mathbf{N}_\alpha \boldsymbol{s}.\boldsymbol{q}\mathrm{d}\Omega - \oint_\Gamma \mathbf{N}_\alpha(\mathbb{F}_j.\boldsymbol{q}).\boldsymbol{n}\mathrm{d}\Gamma + \int_\Omega \mathbf{N}_\alpha \mathbb{R}\mathrm{d}\Omega. \tag{5}$$

In DG methods the solution can be discontinuous from one element to the other. Moreover, the surface integral of equation (5) is computed from the solutions on both sides of the element ensuring a good stability of the numerical method. One of the strengths of the variational formulation presented in equation (5) is that using an explicit time discretization, the linear system becomes block diagonal.

Therefore, the linear system inversions at each time step may be avoided and it can be replaced by matrix multiplications. In addition, the last term of equation (5) represents the volume sources applied to the momentum equation. Since the acoustics (5-l.h.s) and aerodynamic sources (5-r.h.s) are very disparate in terms of characteristic length, the variability of the source terms is taken into account inside element by the high-order Lagrange shape functions $\mathbf{N}_\alpha$ of the numerical algorithm.

3. Flow solution

The CFD simulation is performed using *OpenFOAM* for the simplified HVAC duct with rectangular cross section which dimensions are expressed in mm as depicted in figure 1a. The domain is represented by a cavity of dimensions $2\ \mathtt{m} \times 2\ \mathtt{m} \times 1.6\ \mathtt{m}$ with two main boundary conditions: (i) an inlet boundary condition with constant velocity $U = 7.5\ \mathtt{m/s}$ in one side of the duct; and (ii) outlet boundary conditions (pressure outlet) at each side of the cavity; as depicted in figure 1d. Since the flow is incompressible, the solver selected was *pimpleFOAM*, a large time-step transient solver for incompressible flows based on PIMPLE (merged PISO-SIMPLE) algorithm [21].

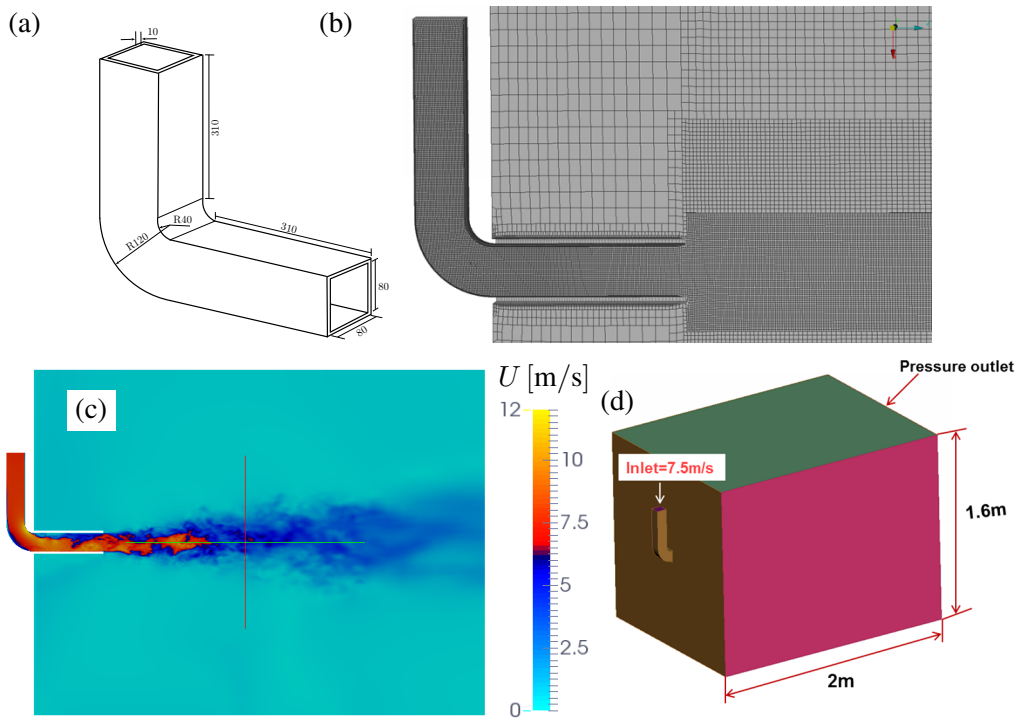

Figure 1: Flow model. (a) Geometry of the simplified HVAC duct, the values are expressed in mm. (b) Detail of mesh used in the CFD simulation near the duct's discharge. (c) Instantaneous norm of the velocity for $t = 0.7\ \mathtt{s}$ computed by the CFD solver. (d) CFD model with boundary conditions and dimensions indicated over the figure.

The fluid is air at standard conditions with constant density $\rho_0 = 1.225\ \mathtt{kg/m^3}$ and kinematic viscosity $\nu = 1.7 \times 10^{-5}\ \mathtt{m^2/s}$. The Reynolds number for the configuration is estimated to exceed $Re = 3.5 \times 10^4$ based on the duct's transverse length $L = 0.08\ \mathtt{m}$. The structured mesh depicted in figure 1b is composed by 3.0×10^6 cells of different sizes: (i) at the boundary layer over the duct walls $\Delta x = 4.5 \times 10^{-4}\ \mathtt{m}$; (ii) in the middle of the duct $\Delta x = 1.0 \times 10^{-3}\ \mathtt{m}$; (iii) at the duct discharge $\Delta x = 3.0 \times 10^{-3}\ \mathtt{m}$; and (iv) near the outer boundaries $\Delta x = 1.5 \times 10^{-2}\ \mathtt{m}$. The simulation was performed from $t_0 = 0\ \mathtt{s}$ to $t_f = 8.5\ \mathtt{s}$ with a time step $\Delta t = 1.0 \times 10^{-5}\ \mathtt{s}$ while the unsteady flow quantities needed for the aeroacoustic simulation where recorded from $t = 0.6\ \mathtt{s}$ until the end of the CFD simulation ($t_f = 8.5\ \mathtt{s}$). For instance, the snapshot of velocity field at $t = 0.7\ \mathtt{s}$ is shown in figure 1c. The Spalart-Allmaras improved DDES (delayed detached eddy simulation) turbulence

model available in *OpenFOAM 2.3.1* was used. The CFD simulation was performed in a cluster of 32 processors *Intel Xeon E3-1240 v2* at 3.40 GHz taking a computation time of 7500 CPU.hr with 1.1 Tb of stored data.

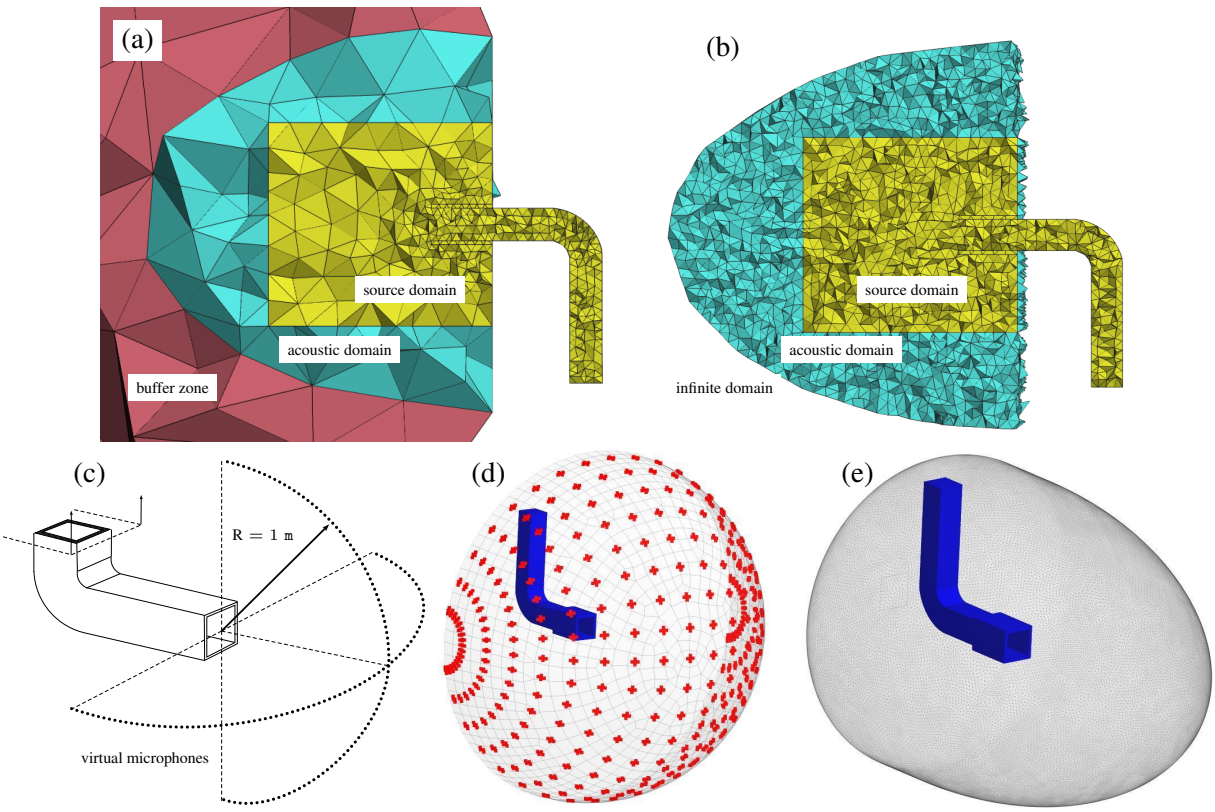

Figure 2: Acoustic model of a rectangular duct. (a) Mesh used in the DG computations. (b) Mesh used in the FE computation. (c) Sketch of the acoustic model with the spherical array of microphones. (d) Array of virtual microphones used in the simulations. (e) Outer surface for computing the sound power.

4. Acoustic models

The acoustic propagation of aerodynamic sources generated by the duct's discharge is now considered. The rectangular duct is immersed in a fluid at rest placed in an anechoic room. As a consequence, the aerodynamic noise produced by the unsteady flow coming out of the duct is the only acoustic source. The fluid media for the propagation of the acoustic waves is assumed homogeneous with constant mass density (same as in the CFD model) and speed of sound $c_0 = 340$ m/s. Two acoustic models are considered: (i) a time domain model solved by means of *ActranDGM* solver and; (ii) a frequency domain model using the implementation of Lighthill's volume sources and solved by means of *Actran* which has been validated [17]. The *ActranDGM* model solves the LEE with source terms in the momentum equation (section §2) using DG method with $p-$adaptivity for the interpolation order inside the element. The mesh used in the *ActranDGM* computation consists in (figure 2a): (i) an acoustic domain corresponding to the duct and the duct's discharge (yellow domain, figure 2a); (ii) a source domain where the acoustic sources are imposed being the same as the previous acoustic domain (yellow domain, figure 2a); (iii) a transition acoustic domain where no sources are applied (turquoise domain, figure 2a); (iv) a buffer zone to damp the sound waves propagated out the physical domain (red domain, figure 2a); and (v) non-reflecting boundary conditions surrounding the buffer zone and the end of the duct. All the domains necessary for the above model form a mesh of 18366 3D-Tetrahedra with 510 2D-Triangular elements. On the other hand, the *Actran* model solves

Lighthill's acoustic analogy in frequency domain as follows:

$$\frac{\partial^2 \rho}{\partial t^2} - c_0^2 \frac{\partial^2 \rho}{\partial x_i \partial x_i} = \frac{\partial^2 \mathbf{T}_{ij}}{\partial x_i \partial x_j}, \qquad \mathbf{T}_{ij} \simeq \rho_0 v_i v_j, \tag{6a,b}$$

with acoustic disturbances having harmonic time dependency $\exp(i\omega t)$, $\omega = 2\pi f$ being the angular frequency. The numerical technique used this time is the classic FE method. The acoustic mesh used in the FE method is more refined because no $p-$adaptivity is used (figure 2b). As an illustration, the FE mesh contains the following domains: (i/ii) acoustic and source domains corresponding to the duct and the duct's discharge (yellow domain, figure 2b); (iii) an acoustic domain for transition where no sources are applied (turquoise domain, figure 2b) contoured by; (v) a domain supporting a non-reflecting boundary condition (infinite elements [20]). The aforementioned domains form a quadratic mesh of 266820 3D-Tetrahedra with 10232 2D-Triangular elements. Besides, the difference in the number of elements between the DG method ($\sim$ 18000) and the FE method ($\sim$ 260000) is notable, this is because, the DG method is based on $p-$adaptivity and at least an interpolation of sixth order is used to assure quality in the solution; instead the FE method is sufficiently refined to use only a quadratic interpolation in the elements. A mesh convergence analysis has been done in each model to assure that the meshes do not need to be refined further. Both acoustic meshes (figures 2a,b) are designed to solve frequencies up to 3 KHz. The degrees of freedom for the *ActranDGM* model rise up to $N_{dof} = 6.53 \times 10^6$ for the maximal frequency in contrast to the *Actran* model having $N_{dof} = 7.55 \times 10^5$ for all frequencies. Finally, it is reasonable to think that the computed sources are less reliable when the CFD mesh coarsens. Therefore, a spatial filter has been used to mitigate the truncation effects at the end of the zone where the CFD results are converted into sources; and to remove the sources computed from coarse CFD cells (far from the duct's discharge). A relative independence of the position of this filter has been observed in additional investigations performed (not presented here).

5. Results and comparisons

The broadband computations on both models (figures 2a,b) are performed in a frequency range from 10 Hz to 2000 Hz with a step of 10 Hz. The average pressure in dB ($p_{ref} = 2 \times 10^{-5}$ Pa) is computed from a spherical collection of 1445 virtual microphones placed outside the source region (far field) at 1 m from the duct discharge (figures 2c,d). In addition, the sound power was also computed (dB, $W_{ref} = 1 \times 10^{-12}$ W) in a surface surrounding the duct discharge (figure 2e) as the surface integral of the acoustic intensity $\mathbf{I} = \frac{1}{2} p\, \mathbf{v}^*$.

In figure 3a, an excellent agreement is found between the *ActranDGM* model, represented as momentum sources in the LEE (red line), and the numerical reference, *Actran* model, represented by Lighthill's analogy (black line). The noise generated by the duct is predominant at lower frequencies (50 Hz - 500 Hz) and rapidly decay as the frequency increases for both numerical models. A similar behaviour is observed for the sound power emission in figure 3b, for *ActranDGM* (red line) and *Actran* (black line). The sound power emission as quadratic indicator behaves as the acoustic pressure, i.e. mostly predominant at lower with a rapid decay at higher frequencies. Few maps illustrating the real part of the acoustic pressure are depicted in figures 4a-h for 100, 500, 1000 and 2000 Hz. The *ActranDGM* (figures 4a-d) and *Actran* (figures 4e-h) models present the same pressure patterns outside the source zone, while inside, the patterns are fundamentally different. Such difference is due to the the source term used in each model. In one hand, the *Actran* model uses the second derivative of Lighthill's tensor $\partial^2 \mathbf{T}_{ij} / \partial x_i \partial x_j$ (scalar) emitting pure acoustic waves (non-rotational). On the other hand, the *ActranDGM* model uses the first derivative of Reynolds' tensor $\partial \rho u_i u_j / \partial x_i$ (vector) as sources emitting both acoustic (non-rotational) and hydrodynamic-vortical (pure rotational) waves, where the former reach the far field.

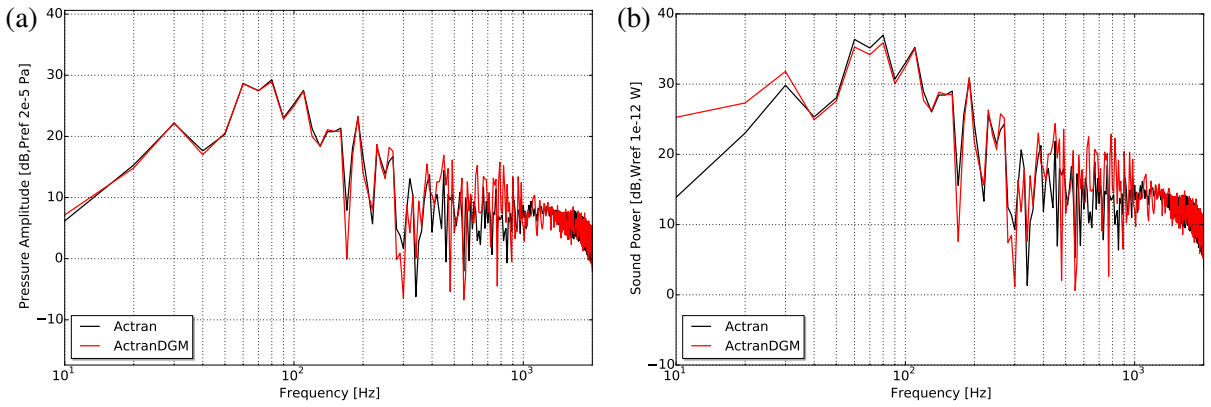

Figure 3: Broadband noise spectra. (a) Average pressure over a spherical collection of microphones computed by *ActranDGM* model (red line) and *Actran* model (black line). (b) Sound power emission computed on a surrounding surface (figure 2e) for *ActranDGM* (red line) and *Actran* model (black line).

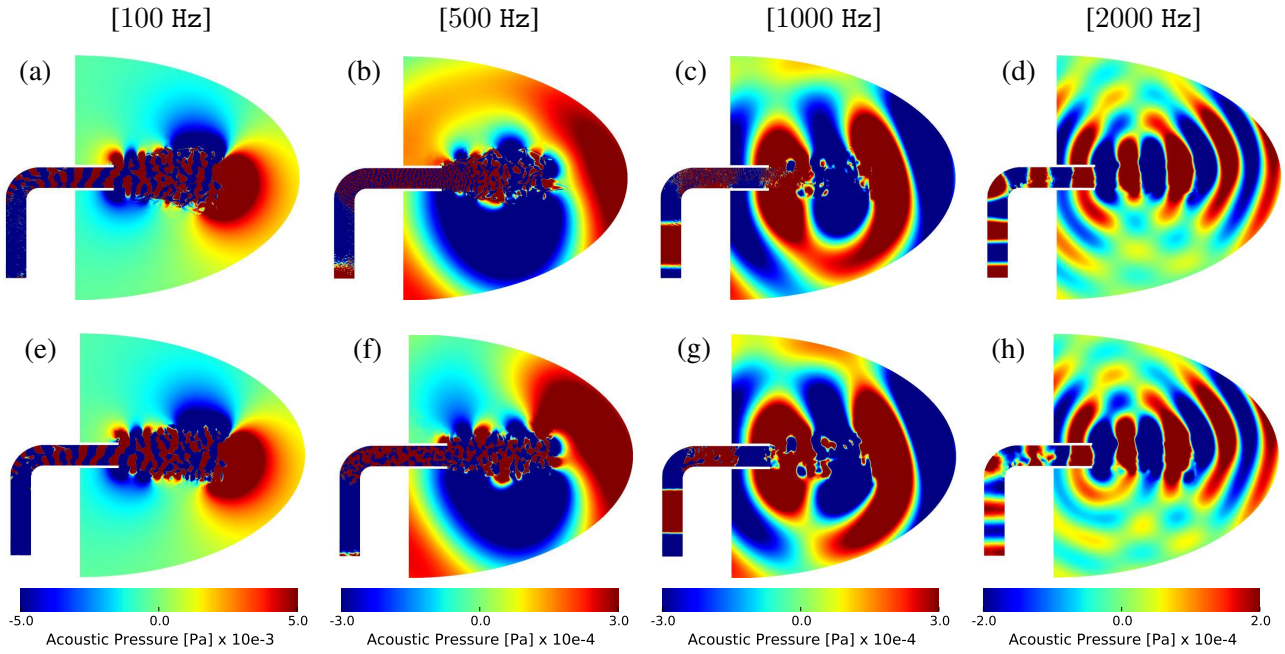

Figure 4: Real part of the acoustic pressure computed by *ActranDGM* (a-d) and *Actran* (e-h) for 100, 500, 1000 and 2000 Hz.

Some comments about the computational time and memory consumption are finally addressed. The acoustic computations corresponding to the *ActranDGM* model were performed in 2 GPU accelerators *Nvidia Tesla K80* (domain parallelism) taking in average 1800 s (total time 1d4h20m) with 3.2 Gb of memory consumption per case. It is noticeable the low memory consumption of the DG method to solve the LEE (1-l.h.s) in time domain, this is one of the features that renders DG methods suitable to acoustic problems in large domains and high frequency. Additionally, the current implementation of aerodynamic sources in *ActranDGM* solver allows parallel computations in multiple CPUs using MPI communicators (not presented here). Loading several sources at different frequencies is not available at the time of performing these investigations but planned for a short term future, leading to a significant reduction of the total computational time.

6. Concluding Remarks

A novel methodology for the computation of aerodynamic sound implemented in a high-order DG method context has been presented. The aerodynamic sources are imposed in time domain on the right-hand side of the LEE as momentum sources, and calculated from unsteady CFD data (hybrid approach). Such sources are mapped inside the high-order acoustic elements to accurately represent the physical phenomena. Moreover, one may mention the advantages of the present method: (i) the numerical method used (DG) has high parallel scalability suited to large acoustic problems and high frequency; (ii) the physical model used (LEE combined with sources) paves the way towards more complete acoustic analogies; a rich variety of sources terms, i.e. mass, momentum and energy sources, convected in a inhomogeneous medium with complex propagation phenomena, i.e. classic flow convection, temperature and mean vorticity effects (shear layers). Finally, future work includes the modelling of sound generated aerodynamically in large industrial applications such as side-mirror noise in cars or pantograph noise in high-speed trains.

REFERENCES

1. Lighthill, M. J. 1952. *On sound generated aerodynamically. I.* General theory. P. Roy. Soc. (London) A-Math. Ph., 211(1107), 564-587.
2. Lighthill, M. J. 1954. *On sound generated aerodynamically. II*. Turbulence as a source of sound. P. Roy. Soc. (London) A-Math. Ph., 222(1148), 1-32.
3. Doak, P. E. 1998. *Fluctuating total enthalpy as the basic generalized acoustic field.* Theoretical and Computational Fluid Dynamics, 10(1-4), 115-133.
4. Curle, N. 1955. *The influence of solid boundaries upon aerodynamic sound.* P. Roy. Soc. (London) A-Math. Ph., 231(1187), 505-514.
5. Williams, J. F., & Hawkings, D. L. 1969. *Sound generation by turbulence and surfaces in arbitrary motion.* Phil. Tran. Roy. Soc. of Lon. A. 264(1151), 321-342.
6. Ribner, H.S. 1959. *New Theory of Jet Noise Generation, Directionality and Spectra*. The Journal of the Acoustical Society of America, 31(2), 245-246.
7. Lilley, G.M. 1974. *On the noise from air jets*. Aeronautical Research Council ARC 20376, U.K.
8. Howe, M. S. 1975. *Contributions to the theory of aerodynamic sound, with application to excess jet noise and the theory of the flute.* J. Fluid Mech., 71(04), 625-673.
9. Möhring, W. 1999. *A well posed acoustic analogy based on a moving acoustic medium*. In Proceedings of Aeroacoustic Workshop Eds. by P. Költzsch, N. Kalitzin.
10. Farassat, F., & Kenneth S, B. 1988. *The uses and abuses of the acoustic analogy in helicopter rotor noise prediction*. Journal of the American Helicopter Society 33, 29-36.
11. Bogey, C., Bailly, C., & Juvé, D. 2002. *Computation of flow noise using source terms in linearized Euler's equations*. AIAA journal, 40(2), 235-243.
12. Billson, M., Eriksson, L. E., & Davidson, L. (2005). *Acoustic source terms for the linearized Euler equations in conservative form.* AIAA journal, 43(4), 752-759.
13. Goldstein, M. E. 2003. *A generalized acoustic analogy.* J. Fluid Mech., 488, 315-333.
14. Ewert, R., & Schröder, W. 2003. *Acoustic perturbation equations based on flow decomposition via source filtering.* Journal of Computational Physics, 188(2), 365-398.
15. Chevaugeon, N., Remacle, J. F., Gallez, X., Ploumhans, P., & Caro, S. 2005. *Efficient discontinuous Galerkin methods for solving acoustic problems.* In 11th AIAA/CEAS Aeroacoustics Conference (p. 2823).
16. Jaeger, A *et al. 2008. Numerical and Experimental Investigations of the Noise Generated by a Flap in a Simplified HVAC duct.* AIAA Paper, 2902, 2008.
17. Caro, S., Detandt, Y., Manera, J., Toppinga, R., & Mendonça, F. 2009. *Validation of a New Hybrid CAA strategy and Application to the Noise Generated by a Flap in a Simplified HVAC Duct.* AIAA Paper, 9.
18. Campos, L. M. B. C., and P. G. T. A. Serrão. *On the discrete and continuous spectrum of acoustic-vortical waves.* International Journal of Aeroacoustics 12.7-8 (2013): 743-782.
19. Legendre, C. *On the interactions of sound waves and vortices*. Ph.d. thesis. Université Libre de Bruxelles 2015.
20. Astley, R. J., and J-P. Coyette. *Conditioning of infinite element schemes for wave problems.* Communications in Numerical Methods in Engineering 17, no. 1 (2001): 31-41.
21. Weller, H. G., Tabor, G., Jasak, H., & Fureby, C. (1998). *A tensorial approach to computational continuum mechanics using object-oriented techniques.* Computers in physics, 12(6), 620-631.
22. Free Field Technologies S.A. 2015. *Actran 16.0 User's Manual*.